8-1-2016

Variable Response of a Thermally Tuned MEMS Pressure Sensor

Robert A. Lake
Air Force Institute of Technology

Ronald A. Coutu Jr.
Air Force Institute of Technology

Recommended Citation

Lake, R. A., & Coutu, R. A. (2016). Variable response of a thermally tuned MEMS pressure sensor. Sensors and Actuators A: Physical, 246, 156–162. https://doi.org/10.1016/j.sna.2016.05.018. https://doi.org/10.1016/j.sna.2016.05.018

Sensors and Actuators A 246 (2016) 156–162

Contents lists available at ScienceDirect

Sensors and Actuators A: Physical

journal homepage: www.elsevier.com/locate/sna

Variable response of a thermally tuned MEMS pressure sensor☆

Robert A. Lake*, Ronald A. Coutu Jr.

Department of Electrical and Computer Engineering, Air Force Institute of Technology 2950 Hobson Way, Wright Patterson Air Force Base, OH 45433, United States

ARTICLE INFO

Article history:
Received 18 December 2015
Received in revised form 9 May 2016
Accepted 9 May 2016
Available online 10 May 2016

Keywords:
MEMS
Buckled membranes
Tunable pressure sensors

ABSTRACT

A typical microelectromechanical systems (MEMS) pressure sensor consists of a thin, deformable membrane and sensing element such as a piezoresistive element which is used to measure the amount of deflection in response to an applied pressure. Previous efforts demonstrated that buckled membranes, from silicon on insulator (SOI) wafers, can be thermally tuned via joule heating. By applying heat to the membrane through a resistive heating element, compressive stress is induced in the membrane causing it to buckle further out of plane and increasing its overall stiffness response. It is demonstrated that by increasing the stiffness of the membrane, the response to an increase in pressure can be varied and its overall sensitivity to pressure can be reduced by up to 62%.

1. Introduction

Microelectromechanical Systems (MEMS) buckled membranes are used in a wide range of applications from stiffness tuning, contact actuation, pressure actuation, and pressure sensing. Buckling can be an undesirable failure mechanism in some mechanical structures, however, the ability of MEMS membranes to buckle under compressive stress provides some advantageous characteristics. A buckled membrane can be treated as a spring that will exhibit regions of positive and negative stiffness depending on its deflection due to its internal energy. The mechanical characteristics, particularly the stiffness, are demonstrated to be tunable. With the introduction of additional stress through localized heating, it has been demonstrated that the membrane will increase its initial deflection which, in turn, alters its stiffness.

This paper discusses the design, fabrication, testing, and analysis of SOI microfabricated membranes. Six different membranes were studied, 1.0 mm × 1.0 mm, 1.5 mm × 1.5 mm, and 2.0 mm × 2.0 mm membranes with a thickness of 7 and 8 μm. The stiffness of the membranes is adjusted by localized heating with a resistive heater fabricated on top of the membrane. Voltage applied to this heater causes Joule heating to take place. The heat is conductively transferred to the membrane which causes it to increase in deflection thereby increasing the membranes mechanical stiffness. This increase in mechanical stiffness decreases the pressure sensors sensitivity to applied air pressure on the back side. This decrease in sensitivity is applicable in situations where a "noisy" pressure environment may be present. By decreasing the sensitivity, this pressure noise can be effectively filtered out.

1.1. Background theory

Microfabricated buckled membranes are the heart of this research effort. This section will provide a basic understanding in the relevant theory of the mechanisms used in this study including residual stress and buckling membranes.

1.1.1. Residual stress

Stress develops between the layers of thin films for several reasons. The main cause of this stress is the result of a mismatch in the thermal expansion coefficients and growth procedures [1]. When a thin film is deposited on a thick substrate at elevated temperature and subsequently cooled and operated at an ambient temperature, the difference between the coefficient of thermal expansion (CTE) (α) of the silicon (2.5×10^{-6}/K) and silicon dioxide (0.55×10^{-6}/K) [2,3] induces a residual stress between the layers resulting in a strain of the material.

The strain in a film can be found by applying Eq. (1),

$$\varepsilon = -\Delta\alpha (T_2 - T_1) \quad (1)$$

where ε is the strain, $\Delta\alpha$ is the difference in the thermal expansion coefficients between the two materials, and T_1 and T_2 are the deposition and cooled temperatures respectively. As the materials cool following their deposition process, they begin to contract based

☆ Selected paper from EUROSENSORS 2015 conference, September 6-9, 2015, Freiburg, Germany.

* Corresponding author.
E-mail address: Robert.Lake@afit.edu (R.A. Lake).

http://dx.doi.org/10.1016/j.sna.2016.05.018

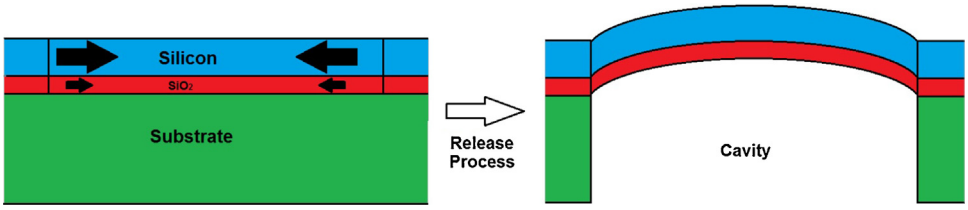

Fig. 1. Illustration of stress induced in the Si/SiO_2 layers as a result of their mismatched thermal expansion coefficients, ultimately leading to buckling upon release [7].

upon their respective CTE. Because the silicon layer has a higher CTE, it wants to contract more than the SiO_2 layer. Since these layers are bonded, a compressive stress is induced in the SiO_2 layer. The silicon layer contains a minimal amount of residual stress because of its higher modulus of elasticity, crystalline structure, and greater thickness compare to the SiO_2 layer [4–6]. This compressive stress causes the membrane to buckle out of plane as illustrated in Fig. 1.

1.1.2. Membrane buckling theory

For a rectangular plate with clamped edges under stress in two perpendicular directions, the expression for the displacement of the buckled membrane at any point (x,y) is given by Eq. (2),

$$w(x,y) = \frac{\delta}{4}\left(1 + cos\frac{2\pi}{a}x\right)\left(1 + \cos\frac{2\pi}{b}y\right) \tag{2}$$

where δ is the vertical deflection at the center of the plate w(0,0), a and b represent the length and width of the membrane [8]. Expressions for the amplitude of the deflection of the buckled plate (δ) under a uniform compressive stress (σ) in two perpendicular directions is given by Eq.n (3) [8,9],

$$\begin{aligned} \delta &= 0 && \text{for : } \sigma < \sigma_{cr} \\ \delta &= \pm 2.298h\sqrt{\frac{\sigma}{\sigma_{cr} - 1}} && \text{for : } \sigma > \sigma_{cr} \end{aligned} \tag{3}$$

where h is the thickness of the membrane and σ_{cr} is the critical stress at which the membrane will begin to buckle. The critical stress of the membrane is given by Eq. (3),

$$\sigma_{cr} = 5.33\frac{\pi^2}{a^2}\frac{D}{h} \tag{4}$$

where a is the length and width of the square membrane and D is the flexural rigidity of the membrane given by Eqs. (5)–(8) where E is the Young's Modulus, and υ is Poisson's ratio [8–10],

$$D = \frac{AC - B^2}{A} \tag{5}$$

$$A = \sum_k \frac{E_k}{1 - \upsilon_k^2}(z_k - z_{k-1}) \tag{6}$$

$$B = \sum_k \frac{E_k}{1 - \upsilon_k^2}\left(\frac{z_k^2 - z_{k-1}^2}{2}\right) \tag{7}$$

$$C = \sum_k \frac{E_k}{1 - \upsilon_k^2}\left(\frac{z_k^3 - z_{k-1}^3}{3}\right) \tag{8}$$

1.2. Fabrication

The fabrication of the tunable pressure sensors requires two main parts, heater fabrication and membrane fabrication. The heaters are fabricated first through an additive process and then the membrane is fabricated by etching through the back of the wafer stopping at the buried oxide layer of the SOI wafer.

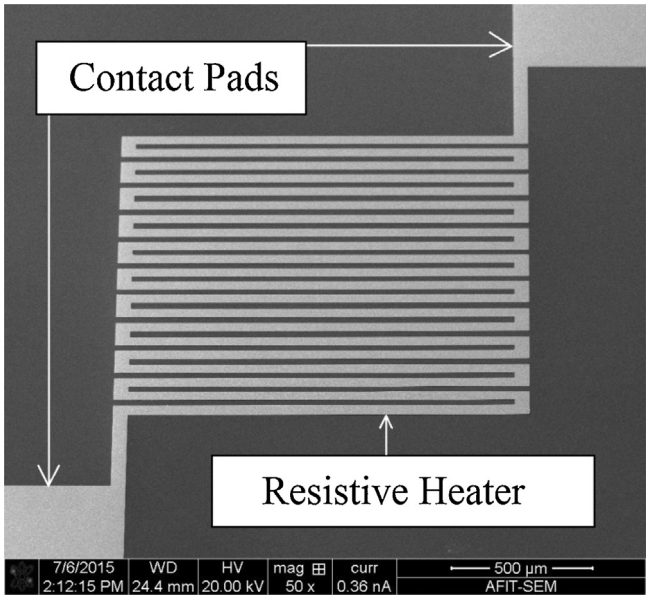

Fig. 2. Scanning electron microscope image of the resistive heater fabricated on top of the membrane. Probes placed in contact with the two contact pads pass current through the meandering resistive heater resulting in Joule heating [7].

1.2.1. Heater fabrication

The stress in the membrane is varied by increasing its temperature. The membrane is heated by a meandering resistive heating element fabricated directly on top of the membrane. The heating element consists of a 3000 Å layer of gold on top of a 500 Å titanium adhesion layer. It was patterned using the liftoff method. The resulting heater is illustrated by Fig. 2.

The sample was first cleaned with a 30 s rinse of acetone, a 30 s rinse of methanol, and a 30 s rinse of DI water and dried with pressurized N_2. A layer of S1818 photoresist was spin coated on to the device layer side of the sample and spun for 30 s at 4000 RPM resulting in a 1.8 μm coating of photoresist. This was then baked at 110 °C for 75 s and then allowed to cool.

The photoresist was then exposed to UV light using a Karl Suss MJB-3 mask aligner for 7 s to provide an exposure dose of 77 mJ/cm^2. Following the exposure, the photoresist was developed in a developer solution of 5:1 DI water to 351 developer for 30 s. Following the development, the sample was rinsed in DI water for 30 s and dried with pressurized N_2.

With the heater now patterned in the photoresist, the samples were placed in a Torr International electron beam evaporation tool. The first layer deposited was a 500 Å thick layer of titanium followed by a 3000 Å thick layer of gold. After the metal deposition, unwanted metal was removed by a liftoff process. The samples were placed in a container of acetone which was placed into an ultrasonic bath. This acetone dissolved the remaining photoresist which removed the metal deposited on top of it, leaving only the resistive heater on the sample.

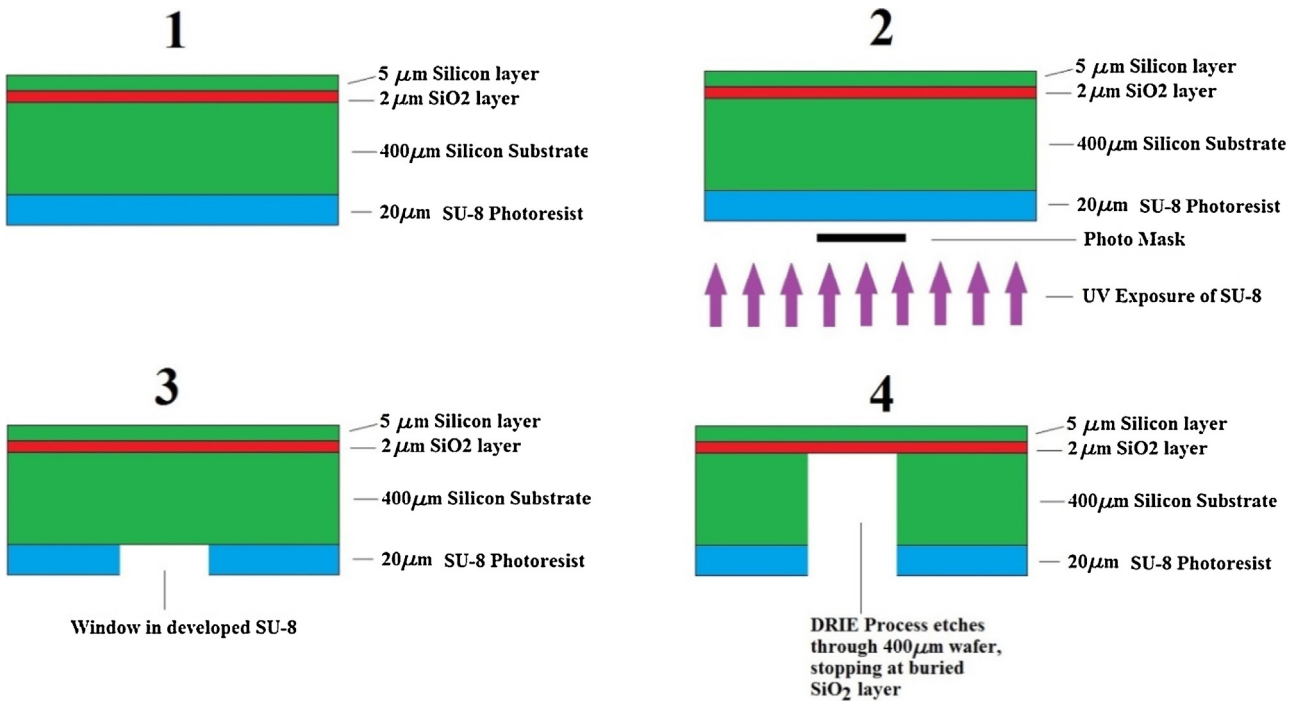

Fig. 3. Step-by-step illustration of the membrane fabrication process. A 20 μm thick layer of SU-8 is deposited on the handle side of a SOI wafer (1). This SU-8 layer is patterned with standard photolithographic technique (2) and developed, leaving a window which exposes the underlying silicon (3). A deep reactive ion etch (DRIE) is performed stopping at the buried oxide layer creating a cavity and releasing the membrane structure (4).

1.2.2. Membrane fabrication

The buckled membrane structures are fabricated on a silicon-on-insulator wafer. The wafers consist of a 500 μm thick silicon handle with a 2 μm thick buried oxide layer of SiO_2 grown on top of the handle layer. A 5 μm or 6 μm thick device layer of silicon is bonded on top of the buried oxide layer. The membranes are released by way of a backside etch through the entire depth of the handle wafer, stopping at the buried SiO_2.

The SOI wafers were first diced into 1 inch by 1 inch square samples for easier processing. Prior to dicing, a protective layer of S1818 photoresist was applied to the front side of the wafer. This layer serves to protect the wafer and heaters from any debris resulting from the dicing process. After dicing, the samples were cleaned with a 30 s acetone rinse, 30 s methanol rinse, and a 30 s DI water rinse and dried with pressurized nitrogen. Finally the samples were placed on a hotplate at 110 °C to evaporate any remaining moisture and then allowed to cool.

A layer of SU-8 photoresist was spin coated at 3000 RPM for 30 s on the handle side of the sample to obtain a 25 μm thick coating of SU-8. Following the spin coating, the samples were soft baked on a 65 °C hotplate for 2 min and then placed on a 95 °C hotplate for 5 min. The samples were then allowed to cool before exposure.

The samples were aligned and exposed with the MJB-3 mask aligner and exposed. The UB power of this tool is set to 11 mW/cm^2. The exposure time was set to 15 s to provide exposure energy of 165 mJ/cm^2 as prescribed by the SU-8 data sheet [11]. Following the exposure, the samples were placed on a 65 °C hotplate for 1 min then placed on a 95 °C hotplate for 5 min for the post exposure bake (PEB). The samples were then developed for 1 min using Microchem's SU-8 developer and then rinsed in DI water. The development opens up the windows in the SU-8 mask layer that will allow the cavity to be etched through the handle to create the membrane structures.

The samples were etched using an STS Pegasus deep reactive ion etching (DRIE) tool. Samples were mounted to a 4 inch carrier wafer and loaded into the tool. The etch rate of the STS Pegasus 4 has been characterized at 15 μm/min so an etch time of 34 min was chosen to etch completely through the 500 μm thick handle. After the etch

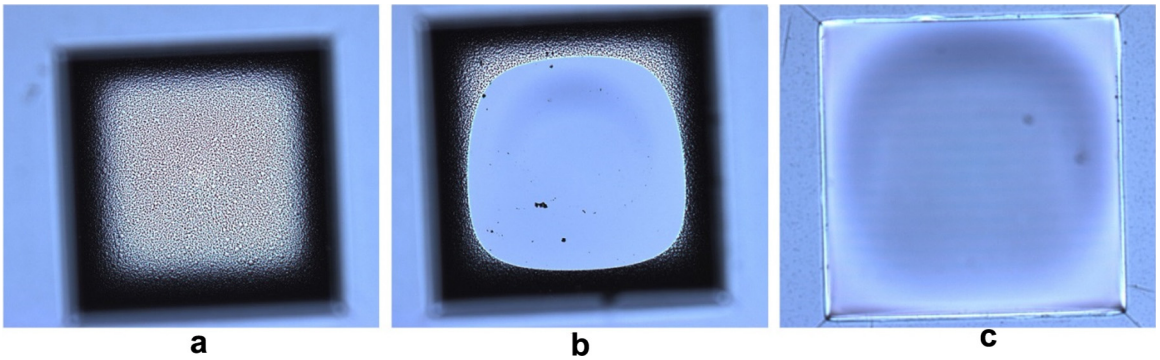

Fig. 4. Optical image of the backside of the membrane post DRIE processing that has not etched completely through to the buried oxide stop layer (a), partially etched through to the buried oxide stop layer, but with some silicon remaining in the corners of the cavity (b), and a completely etched cavity with all silicon completely etched (c).

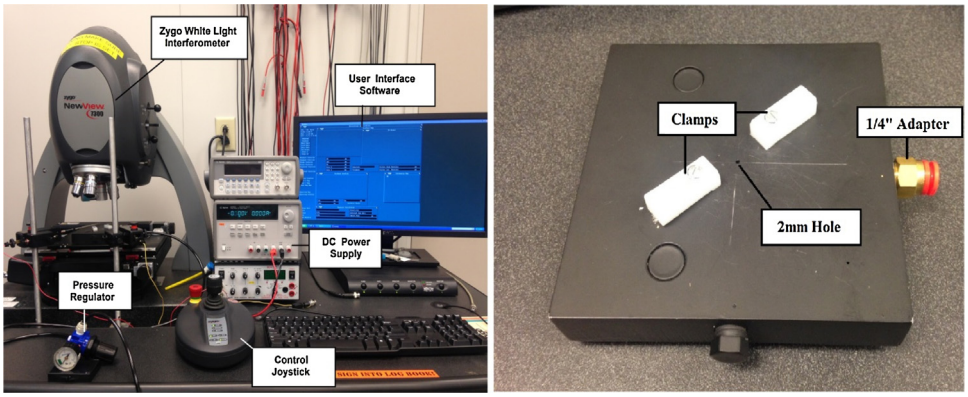

Fig. 5. Complete test set up including Zygo white light interferometer, dc power supply, pressure regulator, and user interface (left.) Specialized test platform to hold samples in place while performing measurements with applied pressure (right) [7].

process was complete, the samples were removed from the carrier wafer and the fabrication steps were complete. This entire process is illustrated in Fig. 3 [7].

It is critical to inspect the backside of the membrane following the DRIE process to ensure that the cavity has been completely etched through to the buried oxide layer. Fig. 4 illustrates three possible results following the DRIE process. The first result illustrated by Fig. 4a is where the etch depth did not reach the buried oxide layer, and the bottom of the cavity is still completely covered with silicon. Visually, the post DRIE silicon is pitted and grey in color. The second possibility is where the etch depth reaches the buried oxide layer, but not completely, leaving behind some silicon in the cavity as illustrated in Fig. 4b. The third possible outcome is where the silicon in the cavity is completely etched. Visually this looks like a smooth blueish layer at the bottom of the cavity with no pitted grey silicon remaining. It is important to ensure a complete etch because any remaining silicon in the cavity will affect the mechanical performance of the membrane.

2. Results

The tuning ability of the pressure sensors was determined by measuring the membrane deflection with respect to an applied pressure while varyingRe applied temperature. It is shown that the increased deflection resulting from the thermal expansion of the membrane alters its mechanical dimensions and therefore alters its mechanical properties. This results in a decreased sensitivity to an applied pressure.

2.1. Measurement and data collection

A Zygo New View 7300 white light interferometer was used to measure membrane deflection. By measuring the deflection of the membrane with different applied pressure and temperature, its mechanical response and sensitivity to applied pressure was characterized. To test the pressure sensors on the Zygo, a specialized platform was fabricated. This platform is a solid square slab of aluminum with a 2 mm hole drilled in the center of the horizontal surface. A second hole is drilled in to the side of the platform which intersects the hole from the horizontal surface. A threaded adapter which accepts a 1/4 inch pressurized N_2 line is threaded into the second hole. This set up directs the pressurized N_2 to the back of the pressure sensor.

On the horizontal surface of the platform are two nylon clamps that are held in place by screws. These clamps keep the pressure sensor from drifting around due to the pressure on their underside as well as ensuring a tight fit between the pressure sensor cavity and the 2 mm hole. An adjustable pressure regulator between the N_2 source and the platform is used to control the pressure applied to the tunable pressure sensor. The complete setup, shown in Fig. 5, makes it possible to measure the deflection of the tunable pressure sensor while adjusting both the temperature of the resistive heater and the applied pressure simultaneously.

With the pressure sensor positioned over the 2 mm hole and the voltage probes placed in contact with the resistive heating element, deflection measurements were then made. The pressure was varied from zero psi to ten psi in 2 psi increments. For each level of pressure, the temperature of the membrane was increased by increasing the DC voltage. The vertical deflection of the center of the membrane was then measured and recorded for each value of pressure, temperature, and each different size and thickness of membrane.

The membrane temperature was measured using a FLIR Systems SC6700 infrared camera. This camera is capable of measuring the temperature of an object within 12 mK. Each membrane was positioned under the camera and a DC voltage was applied to the contact pads of the resistive heaters. The control software was configured to the emissivity of silicon and the average temperature of the silicon membrane was measured and recorded for five points at each voltage increment. The voltage was increased in one volt increments from zero volts up to just before the point where the resistive heater failed (seven volts for the 1.0 mm by 1.0 mm membrane, 10 V for the 1.5 mm by 1.5 mm membrane, and 15 V for the 2.0 by 2.0 mm membrane.)

2.2. Measurement results

In order to quantify the effects of thermal stiffness tuning on the sensitivity of the pressure sensor, the membrane deflection was measured with respect to varying pressure and temperature. The measurements were repeated on four different membranes and averaged for each size and thickness.

Figs. 6a and b show the deflection measurements results for a 1.0 mm × 1.0 mm 7 μm (Fig. 6a) and 8 μm (Fig. 6b) thick membrane over an applied pressure range from zero to 10 psi and a range of applied temperatures from 299.44 K to 315.88 K. Fig. 6c and d show the deflection measurements results for a 1.5 mm × 1.5 mm 7 μm (Fig. 6c) and 8 μm (Fig. 6d) thick membrane over an applied pressure range from zero to ten psi and a range of applied temperatures from 299.44 K to 317.12 K. Fig. 6e and f show the deflection measurements results for a 2.0 mm × 2.0 mm 7 μm (Fig. 6e) and 8 μm (Fig. 6f) thick membrane over an applied pressure range from zero to ten psi and a range of applied temperatures from 299.44 K to 324.11 K.

Considering the deflection vs pressure relationship, we see that the smaller the membrane, the less it deflects for a given pressure

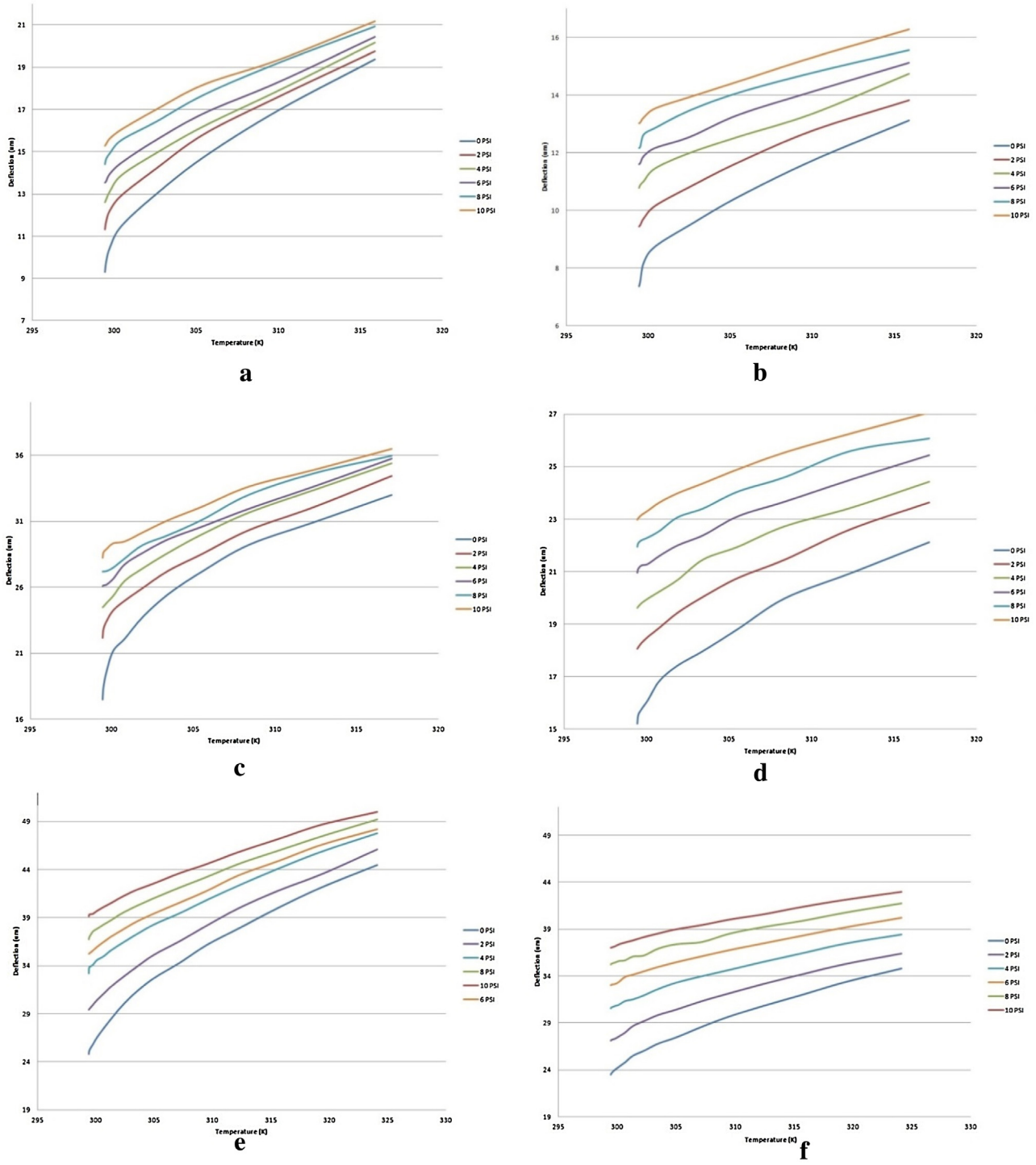

Fig. 6. Plots of the membrane deflection vs applied pressure and temperature. 1.0 mm × 1.0 mm, 7 μm thick (a), 1.0 mm × 1.0 mm 8 μm thick (b), 1.5 mm × 1.5 mm, 7 μm thick (c), 1.5 mm × 1.5 mm, 8 μm thick (d), 2.0 mm × 2.0 mm, 7 μm thick (e), 2.0 mm × 2.0 mm, 8 μm thick (f) [7].

increase. For example, a 1.0 mm × 1.0 mm, 7 μm thick membrane will deflect 6.57 μm from its initial position when 10 psi is applied. The deflection change of each membrane across an applied pressure range of 10 psi is summarized in Table 1.

Looking down the columns of Table 1 and comparing the different sized membranes of the same thickness, we see that as the size of the membrane increases, so does its deflection over a given pressure range. This is attributed to two factors. First, as the membranes increase in size, their overall stiffness decreases, making them less resistant to an applied force. Secondly, as the membranes increase in size, the same amount of pressure on a larger surface area results in greater applied force to the membrane. Looking across the rows

Table 1
Deflection ranges between zero psi and 10 psi for all membranes [7].

	7 μm	8 μm
1.0 mm x 1.0 mm	6.57 μm	5.66 μm
1.5 mm x 1.5 mm	10.73 μm	9.61 μm
2.0 mm x 2.0 mm	14.33 μm	13.56 μm

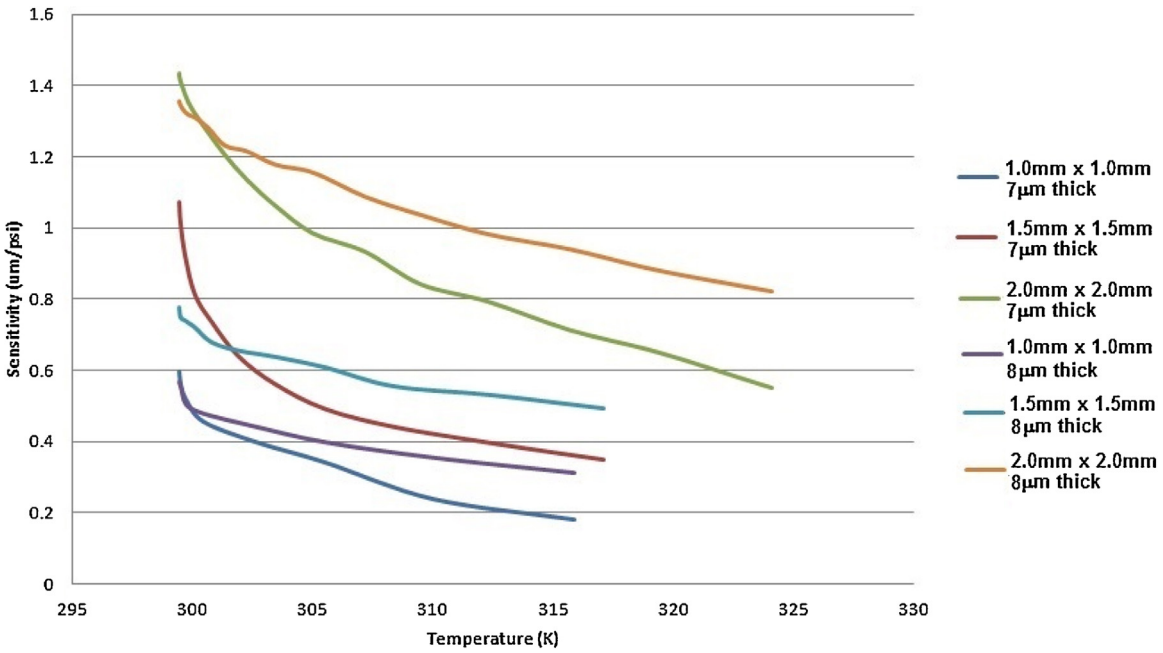

Fig. 7. Plot of the pressure sensitivity vs applied pressure on a 7 μm and 8 μm thick, 1.0 mm × 1.0 mm, 1.5 mm × 1.5 mm, and 2.0 mm × 2.0 mm membrane. The 2.0 mm × 2.0 mm pressure sensor exhibits the widest ranges of sensitivity with the 7 μm thick pressure sensor having the widest of all [7].

Table 2
Deflection ranges over applied temperature range for each membrane [7].

	7 μm	8 μm
1.0 mm x 1.0 mm	8.56 μm	4.89 μm
1.5 mm x 1.5 mm	12.85 μm	7.23 μm
2.0 mm x 2.0 mm	15.76 μm	9.04 μm

of Table 1 and comparing the same sized membranes of different thicknesses, we see that the 8 μm thick membranes deflect less than the 7 μm thick membranes of the same size. This can be directly attributed to the flexural rigidity of the membranes. Looking back at Eqs. (5)–(8) we see that as the thickness of

the membrane is increased, so is its flexural rigidity. This greater flexural rigidity results in thicker membranes having a "flatter" response than a thinner membrane would to the same applied pressure. Membrane temperature vs. deflection results indicate that the smaller the membrane, the less it deflects for a given temperature increase. Table 2 summarizes the change in deflection of each membrane over a given temperature range.

Looking down the columns of Table 2 and comparing the difference sized membrane of the same thickness, we see that as the size of the membrane increases, so does its deflection over a given temperature range. Referring back to the equation for critical stress (Eq. (4)) we see that the critical stress of the membrane decreases as its size increases. According to Eq. (3), as the critical stress decreases with respect to applied stress, the deflection will increase. In other words, a membrane with lower critical stress will deflect more than a membrane with a higher critical stress for the same applied temperature.

Looking across the rows of Table 2, we see that as the thickness increases, the deflection range decreases. Again, referring to the critical stress equation we see that the critical stress of the membrane increases as the flexural rigidity of the membrane increases. The membrane deflection will be smaller for a greater critical stress at the same applied temperature.

The sensitivity of the pressure sensor is the ratio of its deflection to the pressure applied. A pressure sensor that is more sensitive will deflect further than a less sensitive pressure sensor will for the same applied pressure. By thermally tuning the stiffness of the buckled membrane, the sensitivity is also tuned.

The sensitivity was quantified by taking the overall range of the membrane deflection from 0psi to 10 psi with no heat applied and at its maximum applied heat. It can be seen here that while each configuration of pressure sensor has a unique curve, all of them are found to have a decreasing sensitivity over their range of applied temperatures.

The plot of the sensitivity for each membrane over a range of applied temperature is given in Fig. 7. It can be seen that the two pressure sensors made from the 2.0 mm × 2.0 mm membranes have the greatest overall range of sensitivity while the 1.0 mm × 1.0 mm membranes have the least overall range. Additionally, the 8 μm thick pressure sensors exhibit a "flatter" response to applied pressure than that of the 7 μm thick pressure sensors do for the same applied temperature. For each size membrane, there is a cross-over point of the sensitivity response curves. This happens because the thinner membranes will have a greater initial deflection than the thicker membranes have a steeper response curve than their 8 μm thick counterparts.

3. Conclusions

A tunable pressure sensor was designed, fabricated, and characterized. It was found that by electrothermally tuning and increasing the stiffness of a buckled membrane, its sensitivity to an applied pressure is decreased. Typical MEMS pressure sensors based on membranes have a fixed response to pressure that is based on the dimensions and material properties of the membrane. As such, these traditional membranes may be well suited to a particular environment but not applicable in other environments. The pressure sensors presented in this paper resolve this issue by allowing the pressure response of the membrane to be tuned to fit a particular environment. The ability to reduce the pressure sensitivity of these sensors by up to 62% gives it a wider range of application such as in situations where there may be a "noisy" pressure environment present. The ability to selectively adjust the sensitivity of

a pressure sensor will allow this pressure noise to be filtered out of any measurements [7,12].

4. Disclaimer

The views expressed in this paper are those of the authors and do not reflect the official policy or position of the United States Air Force, Department of Defense, or the U.S. Government.

Acknowledgements

The authors wish to thank the AFIT cleanroom technicians for their assistance with this effort. Additionally, thank you to University of Michigan Lurie Nanofabrication Facility.

References

[1] G. Kaltas, A. Nassiopoulo, M. Siakavellas, E. Anastassakis, Stress effect on suspended polycrystalline silicon membranes fabricated by micromachining of porous silicon, Sens. Actuators 68 (1998) 429–434.
[2] J. Laconte, D. Flandre, J. Raskin, Micromachined Thin-Film Sensors for SOI-CMOS Co-integration, 1st edition, Springer, US, 2006.
[3] T. Iida, T. Itoh, D. Noguchi, Y. Takano, Residual lattice strain in the silicon-on-insulator bonded wafers: thermal behavior and formation mechanisms, J. Appl. Phys. 87 (2000) 675–681.
[4] I. De Wolf, Micro-raman spectroscopy to study local mechanical stress in silicon integrated circuits, Semicond. Sci. Technol. 11 (1995) 139–154.
[5] L. Starman, R. Coutu Jr., Using micro-raman spectroscopy to assess MEMS Si/SiO_2, Exp. Mech. 53 (2013) 2174–2179.
[6] S. Best, Detection of Residual Stress in Multi-crystaline Silicon Wafers Using Swept-sine Frequency Response Data, Ph.D Dissertation, University of South Florida, 2005.
[7] R. Lake, Novel Applications of a Thermally Tunable Bistable Buckling Silicon-on-Insulator Microfabricated Membrane, Ph.D Dissertation, Air Force Institute of Technology, 2015.
[8] S.P. Timoshenko, Theory of Elastic Stability, 1st edition, McGraw-Hill, 1961.
[9] D. Popescu, T. Lammerink, M. Elwenspoek, Buckled membranes for microstructures, Proc. IEEE Conference on Microelectromechanical Systems (1994).
[10] R. Szilard, Theories and Applications of Plate Analysis, 1st edition, Wiley, 2004.
[11] SU-8, (2000), Permanent epoxy photoresist processing guidelines, www.microchem.com.
[12] R. Lake, K. Ziegler, R. Coutu Jr., Thermal tuning of a MEMS buckled membrane actuator stiffness, Proc. 28th European Conference on Solid State Transducers (2014).

Biographies

Robert A. Lake received the B.S. degree in electrical engineering from the University of Massachusetts, Lowell, in 2008, the M.S. degree in electrical engineering from the Air Force Institute of Technology (AFIT), Wright-Patterson Air Force Base, OH in 2010, and the Ph.D. degree in electrical engineering from the Air Force Institute of Technology in 2015. He is an Assistant Professor of Electrical Engineering at AFIT. His current research interests are microelectromechanical systems (MEMS), buckled-membrane technology and applications, and solid state microelectronic devices.

Ronald A. Coutu, Jr. received the B.S. degree in electrical engineering from the University of Massachusetts, Amherst, in 1993, the M.S. degree in electrical engineering from California Polytechnic State University, San Luis Obispo, in 1995, and the Ph.D. degree in electrical engineering from the Air Force Institute of Technology (AFIT), Wright-Patterson Air Force Base, OH in 2004. He is an Associate Professor of Electrical Engineering and Cleanroom Director. His current research interests are phase change materials, microelectromechanical systems (MEMS) fabrication and micro-electrical contacts. Prof. Coutu is a registered Professional Engineer, an IEEE and SPIE Senior Member and a Life Member both Tau Beta Pi and Eta Kappa Nu.